THE ASTROPHYSICAL JOURNAL, 389:602–615, 1992 April 20

INFRARED POLARIMETRY AND THE GALACTIC MAGNETIC FIELD. II. IMPROVED MODELS

TERRY JAY JONES, DIMITRI KLEBE, AND JOHN M. DICKEY
University of Minnesota, Department of Astronomy, 116 Church Street SE, Minneapolis, MN 55455
Received 1991 May 20; accepted 1991 October 16

ABSTRACT

The observed trend in interstellar polarization with extinction at 2.2 μm can be well modeled by assuming that interstellar polarization is independent of magnetic field strength and depends only on the geometry of the field. Two models, one invoking Alfvén waves with random phase and one combining ad hoc random and constant components, are developed. The wave model best fits the data when there is equipartition between the magnetic and turbulent energy densities in the ISM. The two-component model best fits the data when there is equal energy in the random and constant components. The observed dispersion in polarization magnitude and position angle requires that the random component of both models decorrelate over an optical depth interval (not physical path length) close to a value of $\Delta\tau \sim 0.1$ at 2.2 μm ($A_V \sim 1$). This constraint on the decorrelation optical depth is found to hold for lines of sight through both the diffuse ISM and dense dark clouds, even though the corresponding physical path lengths are widely different. This suggests that the geometry of the magnetic field is at least partially preserved when molecular clouds contract out of the diffuse ISM. Two simple scenarios for cloud formation, one involving reducing the space between very low filling factor cloudlets and the other involving one-dimensional compression across field lines are discussed.

Subject headings: ISM: general — ISM: magnetic fields — polarization

1. INTRODUCTION

Recently Jones (1989a, hereafter Paper I) found that the magnitude of interstellar polarization measured at K (2.2 μm) is correlated with interstellar extinction. He modeled this trend with a simple vector addition of two components to the magnetic field equal in strength and both in the plane of the sky. One component was constant, and one was random in position angle. The random component was allowed to decorrelate over an optical depth interval at K of $\tau_K \sim 0.1$. While successful, this model required three input parameters, one of which was an arbitrary adjustment of the efficiency at which interstellar dust polarizes light, as well as a dependence of the polarization on magnetic field strength. Jones did not address the observed dispersion in the polarization about his model prediction, nor did he model the observed dispersion in position angle among lines of sight nearby on the sky. Also, Jones did not connect his model with any physical processes taking place in the interstellar medium (ISM).

It is widely recognized that the interstellar medium is clumpy and that turbulent macroscopic motions are often more energetic than microscopic thermal motions (e.g., Dickey 1984). Attempts to relate these turbulent motions to the magnetic field through polarization measurements date back to Chandrasekhar & Fermi (1953), who argued for a connection between the observed dispersion in position angle for stars nearby in the sky and the amplitude of Alfvén waves traveling through the dusty gas responsible for polarizing the light. More recently, Zweibel (1990) extended their treatment to include the degree of ionization and the covering factor. Myers & Goodman (1991) presented a model for the dispersion in position angle that combines a constant and a random component of the magnetic field. In their model both components are free to point in three dimensions and the random component is given a Gaussian distribution in magnitude. They successfully model the dispersion in position angle for several nearby dark clouds.

In this paper we develop a wave model for the magnetic field similar to Chandrasekhar & Fermi and compare its results to observations of the magnitude of the polarization as well as the dispersion in polarization and position angle. We also extend the Myers & Goodman model to include calculations of the magnitude and dispersion of the polarization itself. In § 2 a simple grain model is developed to describe the polarizing power of the ISM as a function of optical depth and direction of the grain alignment. This grain model provides the basic description of how the magnetic field influences the polarization of light by dust. In § 3 we describe the data base available for comparison with our model results. In § 4 our assumptions about the large-scale magnetic field geometry in the galaxy and the way the random component is modeled are presented. The model results are given in § 5 and the implications of these results are discussed in § 6. The details of the grain model and the magnetic field models are placed in the Appendices.

Our goal is to model the *strength* of the polarization as well as the dispersion in the strength and in position angle. Our data base consists of 99 stars with K band polarimetry tabulated in Paper I in addition to more recent observations by Jones (1989b), Klebe & Jones (1990), and Brindle et al. (1991), as well as optical data from Goodman et al. (1990) and the classic paper by Serkowski, Mathewson, & Ford (1975). These data place strong constraints on the relationship between the random and constant components to the magnetic field in the ISM and surprising constraints on the scale length over which the random component decorrelates.

2. GRAIN MODEL

Any model of interstellar polarization requires a description of the polarizing properties of the grains and how they are influenced by the ambient magnetic field. The now classic Davis-Greenstein mechanism has proved to be a useful starting point for models of the grain alignment mechanism. It is highly unlikely, however, that normal paramagnetic relaxation

with thermal spinup of the elongated dust grains is capable of aligning the grains in all phases of the ISM (Chaisson & Vrba 1978; Purcell 1975). The clear presence of well-aligned grains in quiescent, dense, Bok globules for example, argues strongly against normal paramagnetic relaxation (Klebe & Jones 1990; Jones, Hyland, & Bailey 1984). Several nonthermal spinup mechanisms have been devised to enhance the alignment mechanism (see Purcell 1975), however, the interiors of Bok globules are not ideal locations for these mechanisms (Klebe & Jones 1990). So-called superparamagnetic inclusions (SPM) in the grains have been proposed by several authors (e.g., Mathis 1986). These inclusions greatly enhance the dissipation of energy in the spinning dust grain and dramatically speed up the alignment. A very successful and detailed model of the wavelength dependence of interstellar polarization using SPM particles has been developed by Mathis (1986), for example.

Whatever the exact details of the alignment mechanism, it is becoming increasingly clear that the mechanism is very effective, and it aligns the large silicate portion of the total grain population in a time that is short compared to dynamical times in the ISM. For our models we will assume that there is *no* dependence of the net grain alignment on the strength of the magnetic field. In other words, the large elongated component of the grain population is always fully aligned with the ambient magnetic field. With this assumption, the magnitude of the polarization is controlled by the *extinction* (optical depth of the polarizing grains along the line of sight) and the magnetic field *geometry* only. A detailed formulation of the polarizing properties of the grains is given in Appendix A. Here we briefly develop the central characteristics of the model grains.

Following Paper I and Klebe (1989) we describe the polarizing power of the total population of interstellar grains by the parameter η,

$$\eta = \frac{\kappa_\perp}{\kappa_\parallel}, \tag{1}$$

the ratio of the total extinction coefficient perpendicular to the long axis of the aligned component to the total extinction coefficient parallel to the long axis. In this definition, η is less than one, and a smaller η will result in a more highly polarizing medium. For $\eta = 1$ there is no polarization. Note that although η is wavelength dependent, throughout this paper we will only be considering the polarization in the K band, which is centered at 2.2 μm. The differential polarization caused by a uniform slab of dust with thickness dx is then

$$dP = \frac{\kappa_\parallel - \kappa_\perp}{2}\, dx = \frac{1-\eta}{1+\eta}\, \kappa\, dx = \frac{1-\eta}{1+\eta}\, d\tau = d\tau_p, \tag{2}$$

where $\kappa = (\kappa_\parallel + \kappa_\perp)/2$.

Three parameters control the value of η. First is η_p, the value of η for the aligned component of the grains alone. The wavelength dependence of interstellar polarization and the strong interstellar polarization seen in the silicate absorption band at 9.7 μm demand that only a subpopulation of the total grain population actually aligns in the presence of a magnetic field (Dyck & Lonsdale 1980). The second is the fraction of the total extinction the aligned component represents, since not all of the grain population is aligned or contributes to the net polarization. Even if the aligned component were highly polarizing (infinite cylinders), the net polarization would be very low if this aligned grain component constituted a negligible fraction of the total extinction. The third parameter is the angle between the line of sight and the magnetic field direction. If the magnetic field is pointing directly along the line of sight, no polarization will result. If the field lies completely in the plane of the sky, then maximum polarization will result. In Appendix A we show that these parameters result in the following expression for η

$$\eta(\theta) = \frac{\eta_p + (1-\eta_p)\cos\theta + R}{R}, \tag{3}$$

where R is the ratio of the extinction for the unaligned component to the aligned component and θ is the angle between the line of sight and the magnetic field.

The mean values for R and η_p are not free parameters but are fixed by the observed maximum polarization at different values of extinction (see Serkowski, Mathewson, & Ford 1975; Paper I). The maximum observed polarization at 2.2 μm for any optical depth corresponds to $\eta = 0.875$ (Paper I). Consequently, the allowed values of η_p and R are constrained by setting $\theta = 90°$ in equation (3) (magnetic field in the plane of the sky) and then setting $\eta = 0.875$. Klebe (1989) has shown that variations in η_p and R consistent with $\eta = 0.875$ have negligible effects on model results. Therefore, following Klebe we set $\eta_p = 0.5$ and $R = 3.0$ and consider them to be fixed input parameters to the model.

3. DATA SET

For this study we use polarization data taken in both the optical and infrared. The optical data is the familiar study of Serkowski, Mathewson, & Ford (1975), supplemented by more recent results from Goodman et al. (1990). The infrared data is from the compilation in Paper I with new data from Klebe & Jones (1990). The infrared sample breaks into two categories: polarization of stars in or behind dense molecular clouds, and polarization of stars extinguished primarily by diffuse interstellar clouds. The background sources studied are in most cases selected preferentially for high reddening, so the infrared sample is certainly not a random sample of lines of sight. The optical sample is also biased to high extinction, but not as much so as the infrared. Without some extinction, there can be no polarization. In many cases we have several background sources in and behind the same obscuring complex, which is of great interest for studying the small-scale structure of the magnetic field, although it may be incorrect to consider them independent samples for the statistical study of the large-scale magnetic field pattern.

Looking at the large-scale distribution of our infrared data, it is clear that there is an inordinate concentration of samples at longitudes near 0° and 180°. Of the 99 sources, 66 are within 20° of $l = 0°$ or 180°. This can be seen in Figure 1, which shows the longitude distribution of the infrared sample. In latitude, half of the lines of sight are below $|b| < 2°$ (47 of 99), of the rest, nine are in the range $5.3 > |b| > 2°$, and 43 are in the range $9° < |b| < 24°$. The higher latitude lines of sight are concentrated behind nearby dark clouds such as those in Taurus and Ophiucus. Consequently we have relatively few sources where the general direction of the galactic magnetic field is along the line of sight. Rather, we are strongly weighted to lines of sight where the magnetic field is mostly across the line of sight.

4. GALACTIC MAGNETIC FIELD GEOMETRY

We will not attempt to determine the large-scale structure of the galactic magnetic field from these polarization measure-

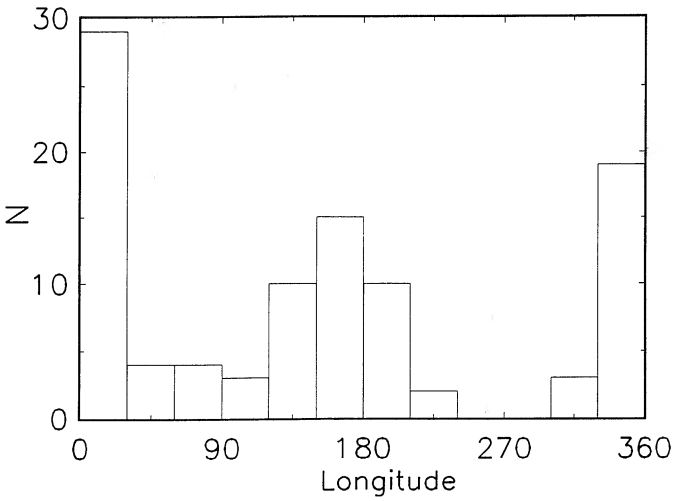

FIG. 1.—The distribution of directions in the galactic plane for the infrared polarization data. Note the concentration of sources toward the galactic center and the anticenter.

ments. This would be inappropriate because of the insensitivity of polarization to magnetic field strength, and because of the limited sampling of the galactic disk by our lines of sight. For the geometry of the ordered component of the magnetic field on a large scale we will simply take the results of rotation measure studies of pulsars and extragalactic sources, Zeeman effect surveys in the 21 cm line, and studies of the polarization of the low-frequency galactic nonthermal background. These and other techniques are reviewed by Sofue, Fujimoto, & Wielebinski (1986), Heiles (1987), Rand & Kulkarni (1989), Valée (1991) and several papers in the volume of Beck, Kronberg, & Wielebinski (1990). In general, these results suggest an azimuthal $\boldsymbol{B}$ field in the galactic plane, with reversals of direction in different radial zones. Whether the local pitch angle is the same as the galactic spiral pattern in the solar neighborhood (13°–15°) or closer to zero is still controversial. Vallée (1991) argues in favor of a 15° local pitch angle and analysis of radio polarization data by Ruzmaiken et al. (1990) suggest a clear departure from a pure azimuthal field in M31. Our data and model are relatively insensitive to differences of 15° or less in the direction of the local magnetic field, but we will consider both cases. Since all of our stars are near the galactic plane, large-scale field geometry above and below the plane is not important for this analysis, and we will assume a simple cylindrical pattern.

In addition to the ordered field, many observations suggest a random magnetic field component. The purpose of this study is to investigate the relationship between this random component and the ordered component through polarization data. In Appendix B we describe two models for the magnetic field in the ISM. In one, developed by Klebe (1989) and based on an idea put forth by Chandrasekhar & Fermi (1953) and further developed by Zweibel (1990), the magnetic field is described as a wave. The amplitude of the wave determines the extent to which the magnetic field direction can fluctuate along a line of sight. For larger amplitude waves, the fluctuations are greater and the net polarization is weaker. The single parameter controlling the amplitude of the wave is $V_{\rm rms}/V_{\rm A}$, where $V_{\rm rms}$ is the rms motion of individual clouds of gas and dust attached to the field lines and $V_{\rm A}$ is the Alfvén velocity. $V_{\rm rms}/V_{\rm A} = 1$ is a special case where the energy density in the magnetic field is in equipartition with the kinetic energy density of the moving clouds. If $V_{\rm rms}/V_{\rm A} = 0$, then the field lines are perfectly straight, and the polarization (to first order) linearly increases with optical depth along the line of sight. For large values of $V_{\rm rms}/V_{\rm A}$, the wave amplitude is very large, and the fluctuations in magnetic field direction along the line of sight are also large. The net polarization will be correspondingly lower.

The second model we describe in Appendix B was developed by Myers & Goodman (1991). In this model (hereafter the MG model) the magnetic field is divided into two distinct components, a random and a constant component. The random component is uniformly distributed in angle over 4π sr. The magnitude of the random component is Gaussian distributed about each rectangular coordinate with dispersion $\sigma_{\boldsymbol{B}}$. The primary parameter controlling the behavior of the MG model is the dispersion in the random component divided by the strength of the constant component $\sigma_{\boldsymbol{B}}/\boldsymbol{B}$. This parameter influences the model in a manner similar to the parameter $V_{\rm rms}/V_{\rm A}$ in the wave model. When $\sigma_{\boldsymbol{B}}/\boldsymbol{B} = 1/\sqrt{3} \sim 0.6$ there is equal energy density in the random and constant components of the magnetic field.

The second input parameter for each model is the path length over which the random component of the field decorrelates. The decorrelation length of the random component is one of the most interesting physical parameters which comes out of this analysis. Unfortunately there are no distance measures to the discrete regions of high extinction which cause the polarization of the stars in our data base. We cannot assume that the polarization takes place in a medium which is homogeneous along the line of sight. The extinction and polarization probably occur in a few small regions of high interstellar density whose overall filling factor is very low. We get no information on the magnetic field between these dense regions, and we have little or no knowledge of distances within or between them. What we can determine about the decorrelation of the random field component is not the distance but the optical depth over which it decorrelates. In modeling the polarization along our lines of sight we take not the distance but the optical depth as the independent variable. Knowing the maximum optical depth to the background star, we consider the variation of the magnetic field along the line of sight in intervals of optical depth from the Earth to the star. What we find is a good estimate for the step size $\Delta\tau$ over which the random component decorrelates.

Figure 2 illustrates how important this correlation is. The points are the measured values of polarization versus optical depth at K (2.2 μm) compiled by Jones. The upper solid line is the dependence of polarization on optical depth if the magnetic field is in the plane of the sky and $\eta = 0.875$ ($P = \tanh \tau_p$, see § 4 and Paper I). This line represents the maximum polarization possible at any optical depth. It does not fit the bulk of the data, but it does form a good upper bound on the distribution of points. The middle line is a model with no ordered field at all; the magnetic field direction is purely random and decorrelates over an optical depth interval $\Delta\tau = 0.1$. Not only is this line well below the ordered field model, but the slope of this line is less, since now the polarization grows only as the square root of the optical depth (i.e., the number of decorrelation optical depths) as expected for a random process. The decorrelation optical depth, $\Delta\tau$, is critical to determining the level of the lower line; a smaller $\Delta\tau$ will significantly offset the line toward the bottom of the figure. The lower line in Figure 2 is the pure random case for $\Delta\tau = 0.01$. For the fully random prediction to be a good lower bound to the observations requires $\Delta\tau \sim 0.1$.

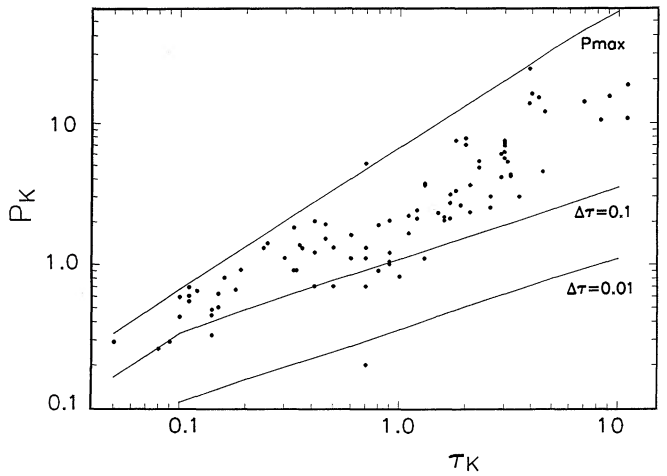

FIG. 2.—K (2.2 μm) band polarization plotted against the optical depth (extinction) at K. The data (*dots*) are from the compilation in Paper I. The upper line is the case for perfect magnetic field geometry, $P = \tanh \tau_p$ (see Jones 1989a). The lower lines are the case for a purely random magnetic field geometry with two values for the optical depth over which the magnetic field loses correlation. Note that the data lies between the purely constant and purely random relations.

The decorrelation scale of the random component of the magnetic field may be astrophysically related to the small-scale structure of the dense phase of the interstellar medium. We are concerned here with the statistics of fluctuations of column density, N, along a given line of sight. N translates into τ_K, the independent variable on Figure 1 using $N_{\rm H\,I} = 2.5 \times 10^{21}$ cm^{-2} A_V (e.g., Dickman 1978) and $\tau_K = 0.09 A_V$. Spectroscopic studies at various wavelengths suggest spatial structure in the interstellar medium on all scales (see Scalo 1990; Wilson 1990; Solomon et al. 1987; Elmegreen 1987). One way to describe this structure is with a "cloud spectrum," $\rho(N)$, which is the probability (per unit line of sight distance) of finding an absorption line of column density N (Dickey & Garwood 1989 and references therein). The model which gives the lower solid line on Figure 2 assumes that all "clouds," i.e., discrete intervals of absorbing material with homogeneous magnetic field direction, have the same optical depth, $\tau_K = 0.1$ ($A_V \sim 1$), corresponding to $N_{\rm H\,I} \sim 2$–3×10^{21} cm^{-2}. This is what would be expected if $\rho(N)$ were a δ-function at the value corresponding to $\tau_K = 0.1$.

A more realistic model for the column density spectrum of the interstellar gas is a power law, $\rho(N) \propto N^{-a}$, extending over several decades in column density. Observations suggest a is in the range 1.5–2.5 for different cloud populations, but we have no knowledge of the smallest discrete column density structures for which this power law holds, i.e., the break in the spectrum $\rho(N)$ on the low side. Presumably it lies somewhere below $N_{\rm H\,I} = 10^{20}$ cm^{-2}, which is roughly the lowest column density absorption line which we can inventory over a large region of the galactic disk, although "neutral clouds" of much smaller optical depths are seen in the halo. This is smaller than the optical depths to the stars in our sample and much smaller than any decorrelation optical depth we can consider. Nevertheless, a power-law distribution for $\Delta\tau$ may be a more realistic description of the range in decorrelation optical depths present in the ISM. At least it will allow us to see what effect a distribution in $\Delta\tau$, as opposed to a single value, will have on the model results.

The observations in Figure 2 clearly lie between $P = \tanh \tau_p$ and the purely random field relation. Thus, a combination of ordered field and random component is needed. This is even more striking if we average the data in several small regions on the sky having several independent sources. These are shown on Figure 3. Here we add two other types of measurements. First are the optical measurements of Serkowski, Mathewson, & Ford (1975) after converting to K band polarization using the Wilking et al. (1982) modification to the Serkowski relation for the wavelength dependence of interstellar polarization. Second are measurements of the aggregate K band polarization and optical depth in the disks of four spiral galaxies, NGC 660 and 992 (Brindle et al. 1991), NGC 3690B (Jones, Gehrz, & Smith 1990), and NGC 4565 (Jones 1989). Starburst galaxies such as NGC 253 and galaxies with active galactic nuclei such as Arp 220 are not included. The average dependence of polarization on optical depth is tightly constrained by these points which clearly lie between the predictions of the perfectly ordered field relation and the random field model. The tightness of the correlation seen in this data, and the clear suggestion of a slope intermediate between those of the two simple models, warrants the construction of more sophisticated models.

5. MODEL RESULTS

In this section we will first assume that the ordered component lies in the plane of the sky for all sources and that a single value for the decorrelation optical depth $\Delta\tau$ defines the decorrelation length for the random component. We then experiment with a power-law distribution for $\rho(\Delta\tau)$ instead of a simple δ-function. Next, we incorporate the assumed global magnetic field geometry of the galaxy into the models. That is, for the ordered component we assume an azimuthal field direction, and take account of the inclination of the ordered field to the line of sight for each star. Finally, we investigate the model predictions for the dispersion in the polarization and the position angle and compare these predictions with the observations.

The model results are computed by dividing up the total

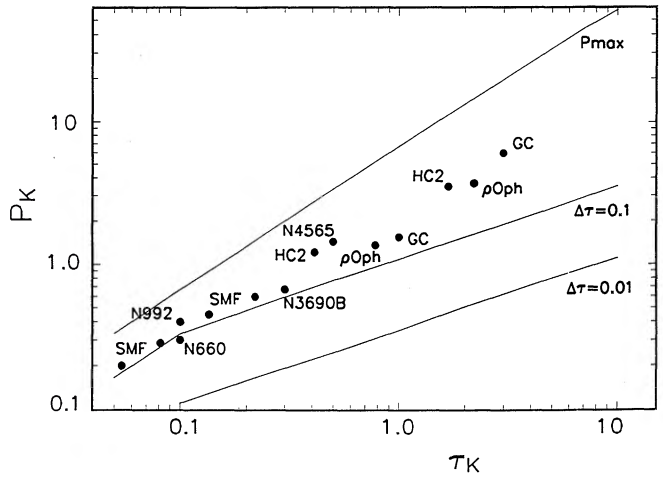

FIG. 3.—Same as Fig. 2 except the individual polarization data has been replaced by the average polarization seen toward several regions in the galaxy at various optical depth intervals. Also included are the polarization measurements of the central regions of several normal spiral galaxies and averages of the optical data in Serkowski, Mathewson, & Ford after conversion to a wavelength of 2.2 μm using the Wilking, Lebofsky, & Rieke (1982) formula. See text.

optical depth of interest into a series of intervals with optical depth $\Delta\tau$. In each interval, the angles θ and θ_p (the projected position angle) are computed based on the magnetic field direction in that interval as determined by the particular choice of model and the values produced by a random number generator. The solutions to the equation of transfer for polarized light given in Paper I (see also Martin 1974 and Nee & Jokipii 1979) are then used to pass the partially polarized light incident from the previous interval through the interval. For the first interval along the line of sight the incident light is, of course, unpolarized. The procedure is continued until the desired total optical depth is accumulated. The model yields a net polarization and a net position angle on the sky for that optical depth (and seed value of the random number generator). The entire set of computations is repeated 10,000 times yielding a mean polarization for the many realizations, a mean position angle (statistically equal to zero), and a distribution of polarizations and position angles about those means. These results are then compared with observational data.

Figure 4*a* shows the results for the wave model for three values of V_{rms}/V_A with $\Delta\tau = 0.1$. Also plotted in Figure 4*a* are the upper bound and the pure random relations shown in Figures 2 and 3. Note that $V_{rms}/V_A = 0$ is equivalent to the upper bound relation and $V_{rms}/V_A = \infty$ is equivalent to the pure random relation. Figure 4*a* clearly shows that a value for V_{rms}/V_A of ~ 1.0 best represents the trend in the data. The model results can be interpreted in simple physical terms. The first model point at $\tau = 0.1$ is below the maximum possible at that optical depth because the magnetic field will not be exactly in the plane of the sky for most of the model realizations when $V_{rms}/V_A > 0$. For the first few decorrelation $\Delta\tau$'s traversed by the light, the effect of different position angles in each interval is to weaken the net polarization compared with a linear trend. This causes the slope of the relation to be significantly less than 1 for $0.1 < \tau_K < 0.5$. At large optical depths the polarization due to the random component, which grows only as the square root of the optical depth, becomes insignificant compared to polarization due to the constant component. The slope of the relation then begins to approach unity.

Smaller values of $\Delta\tau$ cause the relation to shift down and to the left. For this case the model trend returns to a unit slope at smaller optical depths, passing below the data clustered around $\tau_K \sim 0.1$. Larger values of $\Delta\tau$ shift the relation up and to the right. In this case the slope does not depart from unity until larger optical depths. For significant departures from $\Delta\tau = 0.1$ it is more difficult to simultaneously fit the large and small optical depth data. These trends are shown in Figure 4*b* for the wave model with $V_{rms}/V_A = 1.0$. Although the effects in Figure 4*b* of changing $\Delta\tau$ are not large, we will show later that the effect of $\Delta\tau$ on the model dispersion in polarization and position angle are much stronger.

Figure 4*c* shows the results for the MG model for three different values of σ_B/B and $\Delta\tau = 0.1$. The best fit to the data is achieved with $\sigma_B/B = 0.6$, the case for equal energy density in the random and constant components. For $\sigma_B/B = 0$ the upper bound relation is obtained and for $\sigma_B/B = \infty$ the pure random relation is obtained. The effect on the model of changing $\Delta\tau$ is identical to the wave model. Also shown in Figure 4*c* as a dashed line is the wave model for $V_{rms}/V_A = 1.0$, $\Delta\tau = 0.1$ from 4a. Note that the two models are nearly identical when $V_{rms}/V_A = 1$ and $\sigma_B/B = 0.6$. This suggests that the trend in polarization with optical depth can be equally explained by either model. In orther words, passage through a series of combined random and constant components mimics passage through a series of random phase Alfvén waves. For the wave model, the data require that the turbulent and magnetic energy

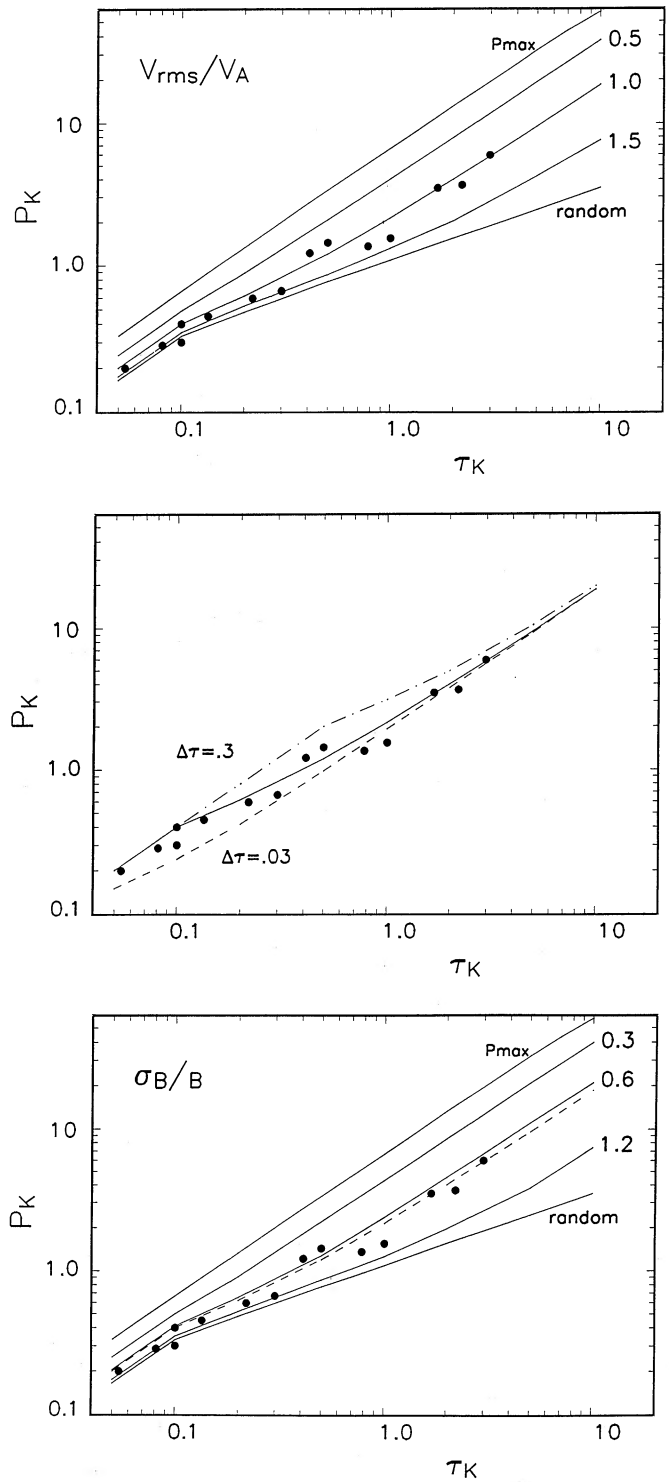

FIG. 4.—Polarization against optical depth for the wave model (*top and middle panel*), and the Myers & Goodman model (*bottom panel*). Top panel model shows results for three values for the parameter V_{rms}/V_A (*solid line:* $\Delta\tau$ = p.1). Middle panel model shows results for three values of the decorrelation optical depth. In the bottom panel, model results for three values of σ_B/B are shown.

density in clouds in the ISM be equal. For the MG model, the data require that the energy density of the random and constant components be equal.

The success of the two models for the simple case of a single value for the decorrelation optical depth is encouraging, but a more realistic distribution for $\Delta\tau$ needs to be investigated. In Figure 5 we show the results of model calculations for a power-law distribution for $\Delta\tau$

$$\rho(\Delta\tau)d(\Delta\tau) = \frac{a-1}{a}\frac{d(\Delta\tau)}{\Delta\tau_0}, \qquad \Delta\tau_0 > \Delta\tau > 0\,; \quad (4)$$

$$\rho(\Delta\tau)d(\Delta\tau) = \frac{a-1}{a}\left(\frac{\Delta\tau}{\Delta\tau_0}\right)^a \frac{d(\Delta\tau)}{\Delta\tau_0}, \qquad \Delta\tau > \Delta\tau_0\,;$$

for three different values of the slope a. In this model, the slope of the $\Delta\tau$ distribution is zero for $\Delta\tau < \Delta\tau_0$. This, in effect causes a break in the power-law distribution at $\Delta\tau = \Delta\tau_0$. A break is necessary to define a lower limit to the rising power law, otherwise the distribution in $\Delta\tau$ will be completely dominated by very small values and produce a poor fit to the data.

In Figure 5 we use the wave model for the magnetic field with $V_{\rm rms}/V_{\rm A} = 1.0$ and $\Delta\tau_0 = 0.1$ for this more complicated distribution for $\Delta\tau$, although the MG model will give nearly identical results. Examination of Figure 5 shows that the effect on the model of different values for the slope is not large, but the data is best fit by the steeper slope (-3). This in effect weights the distribution to values near $\Delta\tau = 0.1$, causing the model to behave in a manner similar to the case for a single value for $\Delta\tau$. Significant changes in the breakpoint $\Delta\tau_0$ result in changes in the model trend very similar to the single value case shown in Figure 4. The effects of changes in $\Delta\tau_0$ on the model dispersion in polarization and position angle are more significant and are discussed later.

The essence of this result is that the power law cannot be too flat, or else occasional very large $\Delta\tau$ steps will raise the predicted polarization above what is observed. Thus, if there is a spectrum of correlation lengths for the magnetic field, it must be a steep spectrum. It is not unreasonable that this spectrum should be steeper than the spectrum of column densities of interstellar absorption lines, since the random component of the magnetic field may vary inside an isolated structure

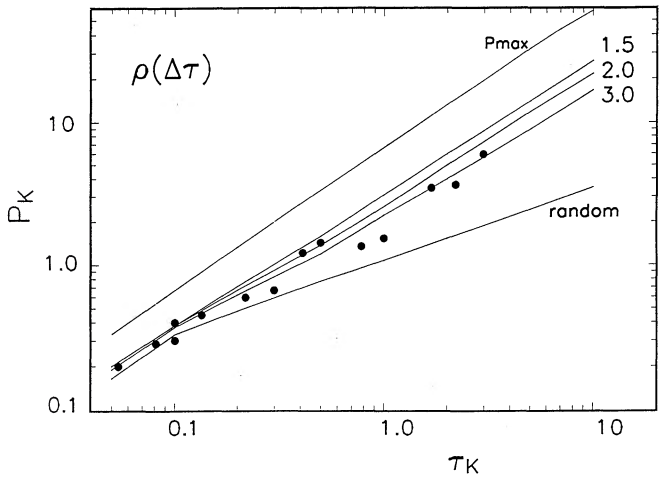

FIG. 5.—Plot of polarization against optical depth for the wave model with a power-law distribution for the decorrelation optical depth $\Delta\tau$. Three values for the exponent $-a$ are shown.

("cloud"). Such small-scale internal structure inside interstellar clouds is detected in both emission and absorption at 21 cm (see Crovisier & Dickey 1983; Kalberla, Schwarz, & Goss 1985; Crovisier, Dickey, & Kazes 1985; Greisen & Liszt 1986 and references therein). The emission studies suggest that the spatial power spectrum of the column density fluctuations lies in the range -2 to -3 (Crovisier & Dickey 1983) or perhaps as high as -4 (Kalberla & Mebold 1983). Thus the value of -3 suggested by our analysis indicates that the small-scale structure of the random component of the magnetic field inside clouds is statistically similar to the small scale structure of the column density.

So far we have assumed that the constant component of the magnetic field lies in the plane of the sky because the majority of our sources lie along lines of sight where this is likely to be the case. We can use the global galactic magnetic field geometry described in § 4 to determine the direction of the constant component along specific lines of sight in the galaxy. By running the model for the line of sight to each source in our sample, we can compute a predicted polarization for each source taking into account the global geometry of the galactic magnetic field. In other words, the galactic field direction is used to determine the angle γ (see Fig. 11, below) in each optical depth interval. We consider two cases, a pure azimuthal field and a field at $l = 75°$ locally. In Figure 6*a* we plot the difference between the observed polarization and the maximum possible polarization ($P = \tanh \tau_p$) divided by the observed polarization for each source in the sample. Note that the data systematically departs from this relation toward higher optical depths. In Figure 6*b*, plotted on the same scale, is the difference between the observed polarization and the MG model with $\sigma_{\boldsymbol{B}}/\boldsymbol{B} = 0.6$ and $\Delta\tau = 0.1$ (single valued) and a pure azimuthal field geometry. The improvement is dramatic and overall the points are well distributed about a difference of zero over the entire range in optical depth. The wave model yields similar results. Most of the improvement is due to the effects of the input parameters to the model, *not* the inclusion of a large-scale galactic field geometry for the constant component. Changing the global magnetic field pitch angle by 15° makes very little difference. This is due to the fact that the random component dominates the net polarization for lines of sight nearly parallel to the constant component of the field.

Scatter about a difference of zero in Figure 6*b* is to be expected since the model prediction represents an average polarization for many statistically independent computations. For each realization of the model a different sequence of random numbers is used to determine the magnetic field geometry in each optical depth interval toward each source. The model prediction is averaging many realizations, but the actual observations represent "single" realizations. All of the models predict that the scatter about the mean model relation as a percentage of the polarization (σ_p/P) should decrease toward higher optical depths (except the pure random case where the ratio remains constant). This is due to the averaging out of the effects of the random component after many optical depth intervals are traversed, resulting in a polarization that is increasingly determined by the constant component alone.

Both the rate at which σ_p/P decreases with increasing optical depth and the magnitude of this ratio depend on the model input parameters. For small values of $\Delta\tau$ the dispersion is smaller than for larger values since there will be more decorrelation intervals for any given optical depth. Large values of $V_{\rm rms}/V_{\rm A}$ or $\sigma_{\boldsymbol{B}}/\boldsymbol{B}$ will cause σ_p/P to drop more slowly with

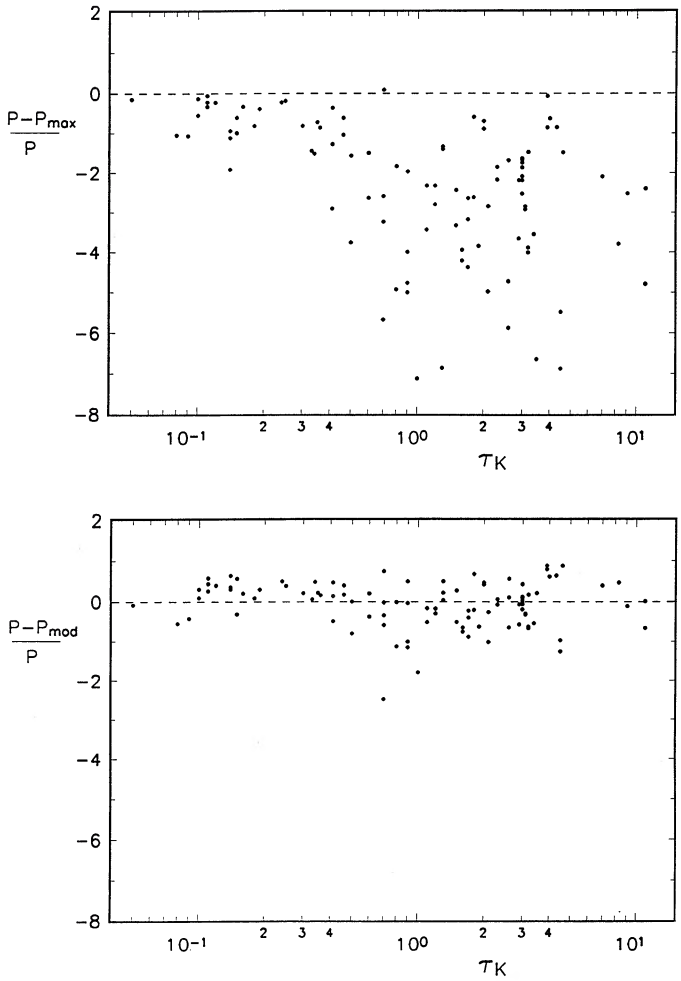

FIG. 6.—*Top panel:* a plot of the difference between the observed polarization P and the model polarization for the constant component only (P_{max}) against optical depth. *Bottom panel:* same as the top panel except the results of the MG model with $\sigma_B/B = 0.6$ and $\Delta\tau = 0.1$. Included in the MG model is the azimuthal geometry of the large-scale magnetic field of the galaxy. Note the improvement over the model without a contribution from a random component.

increasing optical depth. For the pure random case σ_p/P is essentially constant at all optical depths. The exponent in the power-law model for the distribution of $\Delta\tau$ also strongly affects σ_p/P in the sense of shallower slopes producing larger dispersion at large optical depths. This is due to the fact that a shallow slope will allow large optical depths to contain fewer decorrelation intervals on average than would be the case for a distribution more strongly weighted to small values of $\Delta\tau$. Since we have a fairly large sample of polarimetry observations, we can directly compare the model predictions for the dispersion in polarization with the observed dispersion.

In Figure 7 we plot the difference between the observed polarization and the model prediction for the same model parameters as in Figure 6. For this Figure the difference is divided by the dispersion σ_p in polarization predicted by the model, not the observed polarization. The two dotted lines are at $\pm 1\ \sigma$ about a difference of zero. Ideally, the data points would concentrate about zero with approximately one-third of the sources outside the $\pm 1\ \sigma$ borders. In general, this is the case except for a significant number of sources (seven) at high optical depths with polarizations much larger than predicted by the model. These sources are mostly along lines of sight to Cygnus and W3 where the global galactic field is assumed to lie nearly along the line of sight. Consequently the model predicts very low polarization (which is not observed). Along these lines of sight the geometry of the constant component is probably determined by dusty regions near the source and does not closely follow the azimuthal geometry assumed for the galaxy.

The model dispersion grows roughly as the square root of the number of optical depth intervals traversed (due to the random component) whereas the polarization grows faster with optical depth (due to the additional influence of the constant component) and is not as strongly dependent on $\Delta\tau$ (see Fig. 4*b*). Consequently, making the value of $\Delta\tau$ smaller will force more points in Figure 7 to lie outside the $\pm 1\ \sigma$ boundaries due to the correspondingly smaller σ_p in the denominator. For example if $\Delta\tau = 0.03$, $\sim 70\%$ of the data points will lie further than $\pm 1\ \sigma$ from the zero line. Increasing the value of $\Delta\tau$ will, of course, have the opposite effect. For models using a single value for $\Delta\tau$, this parameter must be near a value of 0.1.

Model results using the power-law distribution in $\Delta\tau$ predict a somewhat different behavior in Figure 7. For a steep slope of -3 (and $\Delta\tau_0 = 0.1$), the distribution of $(P - P_{mod})/\sigma_p$ is very similar to the single value ($\Delta\tau = 0.1$) model in Figure 7. For shallow slopes however, the model predicts much larger σ_p at large optical depths. This is due to the higher probability of getting large values of $\Delta\tau$ with a shallow slope. This is turn allows the polarization to be more strongly influenced by the random component at large optical depths than is the case for the models with values for $\Delta\tau$ concentrated near 0.1 where the random component will be mostly averaged out by the time large optical depths are reached. In effect, the divisor σ_p is larger at large optical depths for the case where the exponent is shallower than -3. This will bring the points at large optical depths closer to the zero line in Figure 7. Although this would actually improve the appearance of Figure 7, the effects of a shallow slope for a power-law distribution in $\Delta\tau$ on the dispersion in position angle (discussed next) is at odds with the observations.

Finally, we consider the model predictions for the dispersion

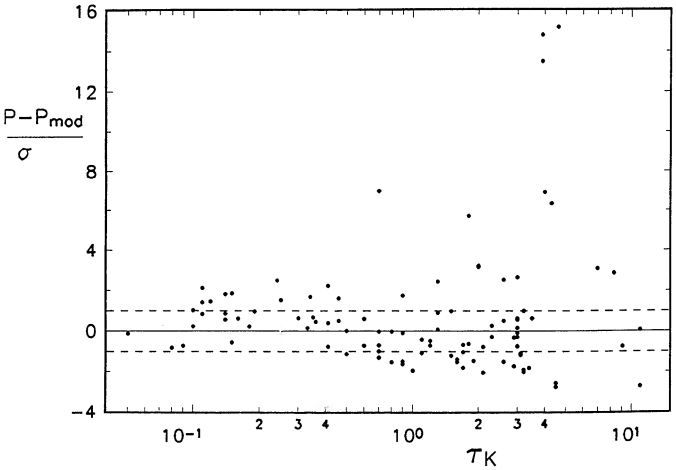

FIG. 7.—Similar to the bottom panel of Fig. 6, except the difference of the observed and model polarizations is divided by the model's predicted dispersion in polarization. The dashed lines are placed at $\pm 1\ \sigma$. Ideally the data would be distributed in a Gaussian manner about the zero line.

in position angle on the sky, σ_θ. Ideally, the data for comparison with the model would consist of statistically independent lines of sight with identical constant component geometry and identical optical depth. This is difficult to achieve since our sample spans a very wide range in constant component geometry and optical depth. As a consequence, we are forced to use observations of sources that are grouped close together in the sky with roughly similar reddening. This is the approach taken by Myers & Goodman, who studied the optical polarimetry of stars shining through nearby dark clouds.

There is some danger in this approach. If the optical depths are large, then presumably many decorrelation intervals are traversed through the cloud. In this case sources nearby in the sky are more likely to be separated by a decorrelation optical depth, assuming the cloud is opaque because it is very dense. For small optical depths through the cloud near the value for $\Delta\tau$, however, this may not be the case. For example, if the optical depth through a dark cloud is equal to $\Delta\tau$ and the cloud is as deep as it is wide, then at most we would be sampling one decorrelation length across the face of the cloud. More than one decorrelation length across the cloud must be sampled if the observed dispersion in position angle is to truly represent the effects of the random component. We will assume that this is the case for all grouped lines of sight in our data base, and we will argue that the large dispersions in position angle seen for stars behind $A_V \sim 1$ ($\tau_K \sim 0.1$) portions of nearby dark clouds demand this assumption.

The model distribution of statistically independent position angles on the sky for the wave model is plotted in Figure 8 for several optical depths with $V_{\rm rms}/V_{\rm A} = 1$ and $\Delta\tau = 0.1$. The narrowing of the predicted distribution in position angle with increasing optical depth is due to the averaging out of the effects of the random component with increasing number of optical depth intervals traversed by the light. The peculiar shape of the distribution for the case of a single optical depth interval is due to the fact that only a single value of $V_{\rm rms}/V_{\rm A}$ is used in the wave model, which tends to cause a peak in θ_p at arctan ($\sqrt{2}$). For the MG model the distribution for the position angle is very similar except that the distribution is much more Gaussian at low optical depths than the wave model. This is due to the fact that the random component is Gaussian

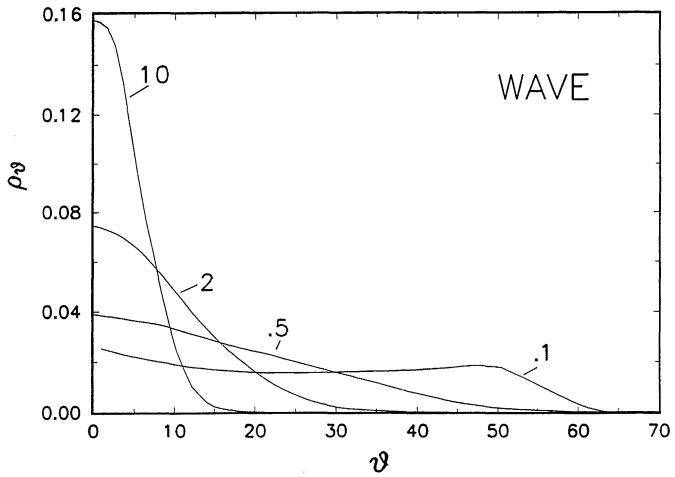

FIG. 8.—The predicted distribution of position angles for the wave model with $V_{\rm rms}/V_{\rm A} = 1.0$ and $\Delta\tau = 0.1$. The numbers next to each curve indicate the total optical depth along the line of sight.

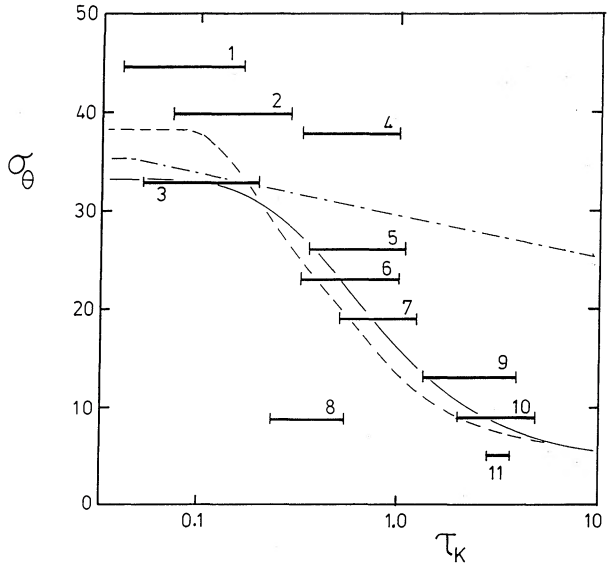

FIG. 9.—Plot of the dispersion in position angle against optical depth. The solid line is the wave model with $V_{\rm rms}/V_{\rm A} = 1$ and $\Delta\tau = 0.1$. The dashed line is the MG model with $\sigma_B/B = 0.6$ and $\Delta\tau = 0.1$. The dot-dashed line is the same wave model but with a power-law distribution for $\Delta\tau$ with a relatively shallow slope of -1.5. The data are as follows: (1, 2, 3): Perseus, ρ Oph, and Taurus; Goodman et al. (1990). (4, 6): B361 and B133; Klebe & Jones (1990). (5): ρ Oph; Wilking et al. (1989). (7): Coal Sack globule No. 2; Jones, Hyland, & Bailey (1984). (8): Heiles Cloud 2; Tamura et al. (1987). (9): ρ Oph; Sato et al. (1988). (10): 100 μm polarimetry of the galactic center; Hildebrand et al. (1990). (11): Galactic center sources; references in Paper I.

distributed to begin with, and there is no tendency for the model position angle to peak at any preferred angle as is the case for the wave model.

In Figure 9 the observed dispersion in position angle for several areas in the galaxy is plotted against the optical depth to the sources. The horizontal bars indicate the range in reddening to the sources. The optical data is taken from Goodman et al. (1990) where we have assumed $\tau_K = 0.09 A_V$. The Bok globule data is from Klebe & Jones (1990) and Jones, Hyland & Bailey (1984). The intermediate optical depth data on ρ Oph is from Wilking et al. (1989), whereas the high optical depth data is from Sato et al. (1988). Only the southern and eastern portion of the region studied by Sato et al. are used. Their data shows an abrupt 90° jump in position angle in the NE. The far-infrared polarimetry of Hildebrand et al. (1990) is used to define one of the galactic center points while the K band data compiled in Paper I is used to determine the other galactic center data point. The polarimetry for Heiles cloud 2 is taken from Tamura et al. (1987).

Also plotted in Figure 9 are the predictions for several of the models. For the wave model, shown as a solid line, $V_{\rm rms}/V_{\rm A} = 1$ and $\Delta\tau = 0.1$. For the MG model, shown as a dashed line, $\sigma_B/B = 0.6$ and $\Delta\tau = 0.1$. The wave model is also plotted for the case where a power-law distribution in $\Delta\tau$ is used. For this model $\Delta\tau_0 = 0.1$ and the exponent is -1.5 (*dot-dashed line*). Steeper exponents cause the power-law version of the wave model to approach the single valued version. Shallow exponents cause the dispersion to remain nearly constant with optical depth, clearly at odds with the data. Note that the value for σ_θ for the wave model at optical depths of only one or two decorrelation depths is not well defined (see Fig. 8).

Overall, the model predictions using $\Delta\tau = 0.1$ are in agreement with the data. An interstellar wind is interacting with Bok

globule B361 (point No. 4 in the Fig. 9) and there are large-scale changes in the geometry of the constant component (Klebe & Jones 1990). Consequently, it shows a larger than predicted dispersion in position angles for the optical depth through the globule. Heiles cloud 2 (point No. 8 in the Fig. 9) is an anomalous region. The location of the data for this region well below the model prediction suggests the magnetic field in Heiles cloud 2 is either very highly ordered or the random component has a very short scale length for decorrelation. If our models are a reasonable description of the magnetic field in the ISM, we must conclude that the magnetic field in Heiles cloud 2 contains an unusually small random component and that the cloud energetics and structure must be dominated by the magnetic field, not the gas motions. Alternatively, the random component varies on very short optical depth intervals ($\sim 1/50$th the optical depth of the cloud!)

The model predictions in Figure 9 are strongly influenced by the input parameters to the models. Values for $\Delta\tau$ much different from 0.1 will cause all of the models to depart from the trend seen in the data in Fig. 9. In particular, smaller values of $\Delta\tau$ will result in dispersions in position angle much smaller than observed in the nearby dark clouds studied in the visual by Goodman et al. (1990). Shallow slopes for the power-law distribution in $\Delta\tau$ strongly flatten out the trend in dispersion with optical depth. Large values for $V_{\rm rms}/V_{\rm A}$ or $\sigma_{\boldsymbol{B}}/\boldsymbol{B}$ will also strongly flatten out the trend in Figure 9 in addition to raising the overall level of the model dispersion. Overall, the observations are best interpreted using a distribution for $\Delta\tau$ peaked near 0.1 and $V_{\rm rms}/V_{\rm A} = 1$ for the wave model or $\sigma_{\boldsymbol{B}}/\boldsymbol{B} = 0.6$ for the MG model.

6. DISCUSSION

Taking the approach of the wave model, the polarization results point strongly to an equipartition situation, where the amplitude of the transverse wave is equal to the amplitude of the ordered, unperturbed field. Following Chandrasekhar & Fermi (1953), this situation corresponds to equipartition between gas pressure and magnetic pressure, since the transverse wave amplitude shows the kinetic energy in random motions of gas. This random motion, which may be identified with turbulence in the interstellar medium, must have kinetic energy equal to the magnetic field energy, $\boldsymbol{B}^2/8\pi$, if the shear wave amplitude is equal to the background field strength. Note that we are referring to the large-scale macroscopic motions in the gas, *not* the microscopic thermal energy, which is usually less (see, for example, Jenkins et al. 1989).

The model with two independent magnetic field components, one perfectly ordered and the other fully random, points to a similar equipartition, but this time between the amplitudes, or energy densities, of the two magnetic field components. At face value this is a statement about the magnetic field geometry and not about the gas pressure or turbulence at all. It is less clear how this model connects to the gas motions in the ISM than with the wave model.

The interaction between fluid motions and magnetic fields in an ionized plasma is a vast subject, and we will not review the theoretical framework here. We take from plasma physics the simple notation of β, the ratio of gas energy density to magnetic field energy density. In place of simple sound waves, three kinds of waves can propagate in a plasma: magnetosonic compressive waves, transverse mode waves, and ion-acoustic waves. In the high β case, the gas turbulence has much more energy than the magnetic field, and so gas motions can tangle the magnetic field into any configuration. In this limit the MG model, independent field components, makes some sense, since there might be no relationship between the random field component, caused by turbulence, and the large-scale ordered field pattern. The tangled magnetic field will gradually try to balance magnetic pressure through the propagation of slow and intermediate waves, but the magnetosonic waves driven by the gas turbulence will constantly disrupt and distort the geometry of the magnetic field. However, for this case we would have $\sigma_{\boldsymbol{B}}/\boldsymbol{B} \gg 1$, which is clearly ruled out by the polarization data.

If β is not large then it is less clear how the MG model for the polarization is tied to the physics of the gas. An arbitrary magnetic field geometry constructed by simply vector adding random components to an ordered component may not even satisfy Maxwell's equations ($\nabla \cdot \boldsymbol{B}$ might be nonzero, for example), let alone reflect patterns to be expected from hydromagnetic turbulence. Many observations in addition to polarimetry suggest that in the Milky Way disk the magnetic field is typically in equipartition with the gas motions ($\beta \sim 1$). So beyond the simple result that the amplitude of the random component must be approximately equal to that of the ordered component, this model may not tell us much about the magnetic turbulence itself.

The wave model is somewhat more physically robust than the independent random component model, but clearly it also represents a simplification of the magnetohydrodynamics. In the solar wind both kinds of compressive wave modes damp rapidly through Landau damping, which may be the case in the interstellar medium as well. A more generalized model including several wave modes would simply introduce more free parameters to the structure of the magnetic turbulence in the interstellar medium. The current data set is inadequate to justify a more detailed formation of the turbulent component.

One important piece of information we obtain from the polarization data is that the correlation length times the density, which we will call the decorrelation column density or optical depth, must be narrowly distributed around $\Delta\tau_K = 0.1$. This is the dust column density needed to give $A_V = 1$. On typical lines of sight through the diffuse ISM in the disk this much dust is encountered in ~ 500 pc of path length (see also Allen & Sukumar 1990 on M83). It is important not to think of the magnetic field geometry as having a decorrelation length of 500 pc, however, since the dust column density is typically dominated by one or more much shorter path lengths through concentrations of interstellar gas and dust. The magnetic field in the intervening sections of the path is not sampled by the polarization data because there is so little dust there. Even for diffuse clouds, the filling factor is typically 5%, so that although the mean opacity at K is $\langle\kappa\rangle = (5\ \mathrm{kpc})^{-1}$, the local opacity inside a diffuse cloud is ~ 20 times higher than this. Thus the typical length along lines of sight in the diffuse ISM which is actually sampled by the polarization data is only ~ 25 pc for each step of $\Delta\tau_K = 0.1$. This may be in a single region or in several spaced along the 500 pc line of sight distance, but the random component of the magnetic field must be aligned throughout.

Many of our lines of sight sample primarily the diffuse interstellar medium, but several molecular cloud regions with very high densities of gas and dust are in our sample as well. These regions give the same result for decorrelation column density as do lines of sight in the diffuse medium, $\Delta\tau_K \sim 0.1$. This is an extraordinary fact, since the line of sight distance for $\tau_K = 0.1$

in cold dense clouds is only a fraction of a parsec. In linear distance it is vastly different from the length through the diffuse interstellar medium, but in terms of column density it is the same.

One interpretation for this apparently remarkable coincidence between the decorrelation column density of the magnetic field in diffuse cloud and dense cloud environments is that it is a consequence of the cloud formation process. The collection and compression of diffuse interstellar matter into a dense cloud must be accompanied by changes in the magnetic field geometry, but some of that geometry must be preserved. What our results show is that the density scales inversely as the first power of the decorrelation length of the field, so as to keep their product constant. In other words,

$$L\rho = \text{constant} , \quad (5)$$

where L is the decorrelation length of the magnetic field.

In the extreme of small β the gas flow is entirely along the magnetic field lines, and the condensation of a cloud might not compress the magnetic field configuration at all. This case corresponds to the formation of a thin pancake and would result in a decorrelation length for the magnetic field that would not change with density. Viewed edge-on (across field lines), such a flattened cloud would have a large optical depth, but no increase in the number of decorrelation intervals. This is certainly ruled out for the interstellar medium by our results.

In the extreme of large β, in a very simple example where a large-scale pressure increase (such as that caused by the gravitational potential of a spiral arm) compresses the gas in three dimensions, the gas pulls the field with it, at least in two dimensions, and perhaps in three dimensions if the field is fairly tangled. In this case the decorrelation length would go roughly as density to the minus one-third power, and so the decorrelation column density would go as density to the two-thirds. This also is ruled out by our results.

We suggest two very simplistic interpretations (neither of them new) to the conclusion that $L\rho$ is narrowly distributed about a single value. One is that the ISM is composed of clouds that behave like beads on strings with a very low filling factor. Compression of the ISM results in the clouds moving closer together, but no compression of individual clouds. Collapse of a larger region under the influence of gravity or interstellar shocks could provide mechanisms for compression. Each cloud preserves its piece of the magnetic field geometry. Thus, compression will increase the bulk density of a region of the ISM, but will not change the optical depth of the individual clouds with their statistically independent random components to the magnetic field. Clearly, this picture must break down at very high densities. At very high optical depths ($\tau_K > 5$) the polarization becomes increasingly less sensitive to the choice of $\Delta\tau$ since so many $\Delta\tau$ intervals will have been traversed.

A second simple picture involves compression in one dimension only of interstellar material *across* field lines (as determined by the constant component). Interstellar shocks, for example, could provide a mechanism for this compression. When viewed across field lines, such structures will have preserved the relationship between decorrelation length and density. When viewed along the field lines, this relationship will not be preserved, but the polarization due to the constant component will be low due to the face on geometry of the spinning dust grains. The polarization along any line of sight primarily down the field lines will be dominated by the random component and those intervals of extinction where the magnetic field is more across the line of sight. Note that our data base is strongly biased to lines of sight primarily across the galactic magnetic field. Also, a randomly oriented cloud will, on average, have a higher probability of having the magnetic field in the plane of the sky than along the line of sight.

It may be that the cloud formation process is largely magnetically driven, so that concentration of the gas is guided by motions of the magnetic field. Perhaps our result that the decorrelation column density is constant reflects a conservation law of some sort in the magnetohydrodynamic turbulence spectrum. This conclusion has similarities to the "condensation law" discussed by Larson (1981). By taking the polarization data, which we have shown is sensitive only to the geometry of the field, in combination with other observations that measure field strength and other components of the geometry, a more comprehensive picture may emerge.

7. CONCLUSIONS

1. The observed trend in polarization with extinction at 2.2 μm can be well modeled by assuming there is no dependence of the polarization on field strength and that the large elongated dust grains are everywhere 100% aligned. The only factors influencing the magnitude of the polarization are the column density of dust and the magnetic field direction along the line of sight. The observed dispersion in position angle in several regions of the galaxy and the observed dispersion in the magnitude of the polarization are also consistent with this conclusion.

2. A model for the magnetic field using Alfvén waves works best when there is equipartition between the magnetic and turbulent energy densities. Departures from equipartition in the model do not reproduce the observed trend of polarization with optical depth, nor do they correctly predict the observed dispersion in polarization magnitude and position angle.

3. A model invoking the vector addition of a constant component and a random component (in three dimensions, Myers & Goodman 1991; see also Paper I) works best when there is equal energy density in the two components. A two-component model with equality between a random and a constant component effectively mimics a model with magnetic waves and equipartition between the magnetic and turbulent energy densities.

4. Both models do a good job of matching the observed dispersion in polarization magnitude and the observed dispersion in position angle. There is some evidence for greater dispersion in polarization at high optical depths than models predict. We suspect this is due principally to dense regions along a few lines of sight with a magnetic field direction very different from the assumed azimuthal field in the disk.

5. The path length over which the magnetic field decorrelates must be tied to the optical depth (column density), not the physical path length. More important, the decorrelation optical depth must be rather narrowly distributed about a value of $\tau_K \sim 0.1$. This corresponds to $A_V \sim 1$ or ~ 500 pc in the diffuse ISM, similar to other determinations of this length in the diffuse ISM by very different techniques (Heiles 1987). Surprisingly, the same value holds for dark clouds as well, even though the physical path lengths are very different. In other words, the density scales inversely with the (physical) decorrelation path length. This suggests that the geometry of the magnetic field is at least partially preserved when molecular clouds contract out of the diffuse ISM.

6. Two simple cloud compression scenarios may explain the dependence of the decorrelation length on optical depth instead of physical path length. One involves clouds that behave like beads on a string with a very low filling factor. Compression will increase the bulk density but will preserve the relationship between optical depth and decorrelation length. This process will break down at very high densities, but our models are not as sensitive to the value of the decorrelation optical depth at very large optical depths. The second involves one-dimensional compression by shocks across field lines. When viewed across field lines, this mechanism will also preserve the relationship between optical depth and decorrelation length. Since our data base is strongly biased to lines of sight across the galactic magnetic field, we are insensitive to lines of sight along the field lines.

APPENDIX A

GRAIN MODEL

Consider a subset of the grain population that is spinning and elongated and therefore capable of being aligned in the presence of a magnetic field. Assume that the time for alignment is short compared to other dynamical times in the ISM. Characterize the polarizing properties of these polarizing grains by the parameter η_p defined as follows:

$$\eta_p = \frac{\kappa_{a\perp}}{\kappa_{a\parallel}} \tag{A1}$$

where $\kappa_{a\parallel}$ and $\kappa_{a\perp}$ are the extinction coefficients of the aligned grains parallel and perpendicular to the long axis of the grains. In this definition η_p is less than one and smaller values of η_p result in larger polarizing power. Most alignment mechanisms orient a spinning elongated grain with the spin axis of the grain perpendicular to the long axis of the grain but parallel to the ambient magnetic field. If the magnetic field is in the plane of the sky, η_p is a minimum (polarizing power is a maximum). If the field direction is along the line of sight, the spinning grains have their axis of rotation pointed directly at (or away from) the observer, resulting in no polarization and $\eta_p = 1$. If we simply model the intermediate case by an ellipse opening up as the grain spin axis is tilted toward the observer (see Fig. 10), then $\eta_p(\theta)$ can be described by the following equation:

$$\eta_p(\theta) = \eta_p + (1 - \eta_p)\cos\theta\ . \tag{A2}$$

The total grain population will have an effective value of η that is closer to 1.0 (weaker) than the aligned component alone since there is no difference between $\kappa_\parallel$ and $\kappa_\perp$ for the unaligned component. Let R be the ratio of the unaligned component to the aligned component.

$$R = \frac{\kappa_u}{\kappa_{a\parallel}} \tag{A3}$$

The extinction for the combination of both components is then

$$\kappa_\perp = \eta_p(\theta)\kappa_{a\parallel} + R\kappa_{a\parallel}\ , \qquad \kappa_\parallel = (1 + R)\kappa_{a\parallel}\ . \tag{A4}$$

Thus the effective η for the total grain population is

$$\eta(\theta) = \frac{\eta_p + (1 - \eta_p)\cos\theta + R}{1 + R}\ . \tag{A5}$$

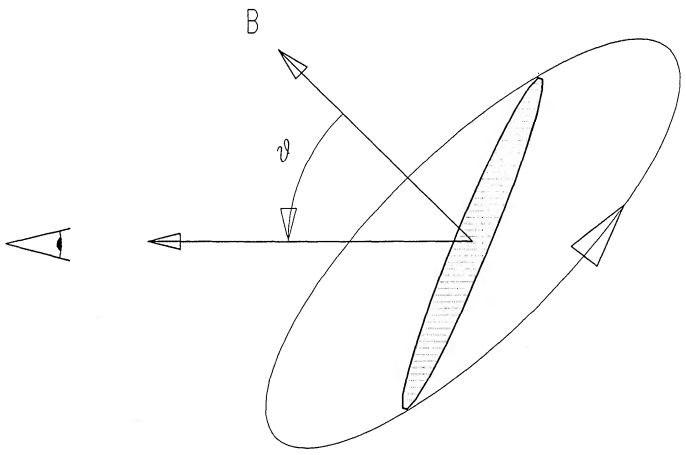

FIG. 10.—Geometric parameters for the grain model

APPENDIX B

1. INTRODUCTION

Jones (1989a, Paper I) proposed a very simple model for the observed trend of interstellar polarization with optical depth that used a constant component and a random component to the magnetic field. In this model a line of sight through the ISM is divided up into individual cells of identical optical depth. In each cell a random magnetic field vector is added to a constant component and partially polarized light from the previous cell is passed through the cell. The light is partially polarized by the cell at the position angle of the net magnetic field. The random component has the effect of causing the position angle of the polarization for each cell to vary along the line of sight. In this way the net effect of passage through several cells will be to polarize the light less than would have been the case for a uniform magnetic field geometry.

This model is flawed in several aspects. First, it places the magnetic field only in the plane of the sky, even though the field can easily point along the line of sight as well as any other direction (§ 4). Second, Jones required the magnitude of the polarization to be linearly dependent on the net magnetic field strength (normalized to the constant component). In § 2 we argued that there is probably *no* dependence of the grain alignment on field strength (at least for the field strengths as strong as those found in the ISM). These two facets of the model forced Jones to arbitrarily adjust the polarizing power of the ISM (the value of η) to obtain a good fit. Also Jones used only a single value for the cell optical depth even though the ISM contains a very complicated range in densities, sizes, and optical depths for the dust distribution. In this section we describe a set of models which eliminates these shortcomings and more closely ties the model input parameters to the physical conditions in the ISM.

Paper I required three input parameters for the model. These were (1) the value for η, (2) the ratio of the constant and random magnetic field components, and (3) the optical depth interval over which the random component changed (the correlation cell). Below we develop two models for the magnetic field geometry in the ISM that will require only two input parameters. These are a measure of the relative strengths of the random and constant components and the decorrelation optical depth.

2. WAVE MODEL

Klebe (1989) modeled the magnetic field geometry in the ISM as a simple Alfvén wave in a manner similar to Chandrasekhar & Fermi (1953) and Zweibel (1990). In this model the ISM is composed of small cloudlets that "ride" on the magnetic field lines. The larger the amplitude of the wave, the larger the velocity of the cloudlets (and vice versa). In this model the random component is embodied in the amplitude of the wave, the greater the amplitude, the greater the variation in the position angle of the magnetic field between locations.

Consider an Alfvén wave traveling in a direction γ with respect to the line of sight. Define the direction of propagation as the local z-axis (see Fig. 11). Define the displacement of the magnetic field from the z-direction as

$$\zeta = A \cos [k(z - V_A t) + \delta] , \tag{A6}$$

where A is the amplitude of the wave, k is the wavenumber, and δ is the phase. The phase δ and the plane of vibration given by the angle ϕ are allowed to be randomly distributed over π and 2π respectively.

Within a cloudlet attached to the wave, the direction of the field line with respect to the z-axis is given by

$$\tan \alpha = \frac{d\zeta}{dz} = -kA \sin [k(z - V_A t) + \delta] . \tag{A7}$$

The velocity of the cloudlet perpendicular to the z-axis is given by the time derivative of ζ

$$V_\zeta = \frac{d\zeta}{dt} = -V_A kA \sin [k(z - V_A t) + \delta] . \tag{A8}$$

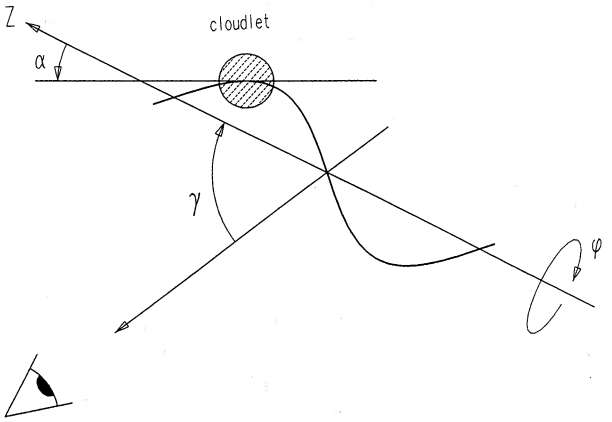

FIG. 11.—Geometry for the wave model

The rms value of this motion is given by

$$V_{\rm rms} = \frac{V_{\rm A}\, kA}{\sqrt{2}} \tag{A9}$$

We can now express α as follows

$$\tan \alpha = \sqrt{2}\, \frac{V_{\rm rms}}{V_{\rm A}} \sin\, [k(z - V_{\rm A}\, t) + \delta]\, . \tag{A10}$$

For any given cloudlet, the angles α, γ, and ϕ define the direction of the magnetic field in that cloudlet with respect to the line of sight (θ in eq. [A5]). They also define the position angle of the magnetic field projected onto the sky (θ_p). In this model each cloudlet along a line of sight is assumed to contain a piece of a wave with a statistically independent phase and plane of vibration. That is, the Alfvén wave in one cloudlet will have the same propagation direction, but will not necessarily have the same phase or plane of vibration as any other cloudlet. Consequently the angles α and ϕ will be statistically independent from cloudlet to cloudlet while γ remains the same.

Note that the range of α is restricted by the ratio of the rms velocity of the cloudlets to the Alfvén wave velocity. This single parameter, $V_{\rm rms}/V_{\rm A}$, defines the ability of the magnetic field to depart from a uniform field direction along a path through the ISM. If $V_{\rm rms}/V_{\rm A} = 0$, then the field line is perfectly straight and the entire path length through several cloudlets will polarize light at the same position angle θ_p and with the same efficiency η. If $V_{\rm rms}/V_{\rm A}$ is large, however, different cloudlets encountered along the line of sight can have very different magnetic field directions, each polarizing the light at a different position angle projected on the sky. The net polarization from such a path will be lower as a consequence.

Also note that even if the propagation vector is in the plane of the sky ($\gamma = 90$), any value of $V_{\rm rms}/V_{\rm A}$ greater than zero will, on average, result in values for θ less than 90. This reduces the polarizing power of the cloudlets through the effect of θ on η in equation (A5). Also θ_p will vary from cloudlet to cloudlet. Thus, on average, the polarization will be lower than the maximum found in the ISM, even when the propagation vector is in the plane of the sky.

In terms of the magnetic field strength $\boldsymbol{B}$ and the mass density ρ, the Alfvén speed is given by

$$V_{\rm A} = \frac{\boldsymbol{B}}{\sqrt{4\pi\rho}}\, . \tag{A11}$$

If we set $V_{\rm rms}/V_{\rm A} = 1$, then we can write equation (A11) as

$$V_{\rm rms}^2 = \frac{\boldsymbol{B}^2}{4\pi\rho} \qquad \text{or} \qquad \frac{1}{2}\, \rho V_{\rm rms}^2 = \frac{\boldsymbol{B}^2}{8\pi}\, . \tag{A12}$$

In other words, when $V_{\rm rms}/V_{\rm A} = 1$ we have equipartition between the magnetic energy density and the kinetic energy density embodied in the motions of an ensemble of cloudlets.

Although we have used the idea of individual cloudlets to describe the path length over which the magnetic field is coherent, we do not imply that the ISM is made up of discrete clouds with sharp boundaries. The cloudlet picture is merely a means of parameterizing the decorrelation length of the random component of the magnetic field. In the main body of the text we explore both a single value for the optical depth of a decorrelation interval and a continuum of decorrelation optical depth intervals.

There are two input variables to this model, the value of $V_{\rm rms}/V_{\rm A}$ and the characteristic optical depth of a single correlation cell $\Delta\tau$.

2. MYERS AND GOODMAN MODEL

Myers & Goodman (1991) describe a model for the magnetic field in the ISM consisting of a fixed component and a random component. The random component is Gaussian distributed in magnitude along three independent rectangular coordinates. Referring to Figure 11, the constant component is a vector along the z-axis. In this model γ is the same as shown in Figure 11, but the angles α and ϕ are now determined by the vector addition of the constant component with the random component. When the energy density of the constant component and the random component are equal, the dispersion of the random component in each axis is

$$\sigma_{\boldsymbol{B}} = \frac{\boldsymbol{B}(\text{const})}{\sqrt{3}}\, . \tag{A13}$$

In this model each decorrelation length for the random component of the magnetic field contains the same constant component of the magnetic field, but a statistically independent random component. The random component for an individual decorrelation length is created by generating a random Gaussian distributed variable for each of three orthogonal directions which in turn define a vector for the random component. This vector is then added to the constant component and the angles θ and θ_p are computed from the sum.

There are two input variables in this model, the dispersion of the random component in units of the constant component $\sigma_{\boldsymbol{B}}/\boldsymbol{B}$(const) and the characteristic optical depth of a correlation cell $\Delta\tau$. Myers & Goodman did not express their model in terms of actual optical depths or use the equation of transfer to compute the magnitude of the polarization. Their principal aim was to model the dispersion in position angle on the sky found in dark cloud complexes. By incorporating our grain model and quantitative optical depths into their model, we are extending the Myers & Goodman model in order to compute the polarization as well.

Paper I modeled the random component as a vector of constant length in only two dimensions with a random position angle in the plane of the sky. Myers & Goodman investigated a similar geometry (their two-dimensional case with a single value for the random component field strength) but found that version of their model to be unsatisfactory. It produced a distribution for the position angle that was a poor fit to the more Gaussian distribution found in several well-studied dark clouds.

REFERENCES

Allen, R. J., & Sukumar, S. 1990, in The Interstellar Medium in External Galaxies: Summaries of Contributed Papers, NASA CP, 3084
Beck, R., Kronberg, P. P., & Wielebinski, R. 1990, IAU Symposium 140, Galactic and Intergalactic Magnetic Fields, in press
Brindle, C., et al. 1991, MNRAS, in press
Chaisson, E. J., & Vrba, F. J. 1978, in Protostars and Planets, ed. T. Gehrels (Tucson: Univ. of Arizona Press), 189
Chandrasekhar, S., & Fermi, E. 1953, ApJ, 118, 113
Crovisier, J., & Dickey, J. M. 1983, A&A, 122, 282
Crovisier, J., Dickey, J. M., & Kazes, I. 1985, A&A, 146, 223
Dickey, J. M. 1984, IAU Symposium 106, The Milky Way as a Galaxy, ed. H. Van Worden (Dordrecht: Reidel), 311
Dickey, J. M., & Garwood, R. W. 1989, ApJ, 341, 201
Dickman, R. L. 1978, ApJS, 37, 407
Dyck, H. M., & Lonsdale, C. J. 1980, IAU Symposium 96, Infrared Astronomy, ed. C. G. Wynn-Williams & D. P. Cruikshank (Dordrecht: Reidel), 223
Elmegreen, D. G. 1987, in Interstellar Processes, ed. D. Hollenbach & H. Thronson (Boston: Reidel), 259
Goodman, A. A., Bastien, P., Myers, P. C., & Menard, F. 1990, ApJ, 359, 363
Greisen, H. S., & Liszt, B. W. 1986, ApJ, 303, 702
Heiles, C. 1987, in Interstellar Processes, ed. D. Hollenbach & H. Thronson (Boston: Reidel), 171
Hildebrand, R. H., Gonatas, D. P., Platt, S. R., Wu, X. D., Davidson, J. A., Werner, M. W., Novak, G., & Morris, M. 1990, ApJ, 362, 114
Jenkins, E. B., Lees, J. F., van Dishoeck, E. F., & Wilcots, E. M. 1989, ApJ, 343, 785
Jones, T. J. 1989a, ApJ, 346, 728 (Paper I)
———. 1989b, AJ, 98, 2062
Jones, T. J., Gehrz, R. D., & Smith, J. 1990, AJ, 99, 1470
Jones, T. J., Hyland, A. R., & Bailey, J. 1984, ApJ, 282, 675
Kalberla, P. M. W., & Mebold, U. 1983, Mitt. Astron. Ges., 58, 101
Kalberla, P. M. W., Schwarz, U. J., & Goss, W. M. 1985, A&A, 144, 27
Klebe, D. I. 1989, thesis, University of Minnesota
Klebe, D. I., & Jones, T. J. 1990, AJ, 99, 638
Larson, R. B. 1981, MNRAS, 194, 809
Martin, P. G. 1974, ApJ, 187, 461
Mathis, J. S. 1986, ApJ, 308, 281
Myers, P. C., & Goodman, A. A. 1991, ApJ, in press
Nee, S. F., & Jokipii, R. J. 1979, ApJ, 234, 140
Purcell, E. M. 1975, in The Dusty Universe, ed. G. B. Field & A. G. W. Cameron (New York: Academic), 155
Rand, R. J., & Kulkarni, S. R. 1989, ApJ, 343, 760
Ruzmaikin, A., Sokoloff, D., Shukurnov, A., & Beck, R. 1990, A&A, 230, 284
Sato, S., Tamura, M., Nagata, T., Kaifu, N., Hough, J., McLean, I. S., Garden, R. P., & Gatley, I. 1988, MNRAS, 230, 321
Scalo, J. 1990, in Physical Processes in Fragmentation and Star Formation, ed. R. Capuzzo-Dodcetta, C. Chiosi, & A. D. Fazio (Dordrecht: Kluwer), 103
Serkowski, K., Mathewson, D. S., & Ford, V. L. 1975, ApJ, 196, 261
Sofue, Y., Fugimoto, M., & Wielebinski, R. 1986, AAR&A, 24, 459
Solomon, P. M., Rivolo, A. R., Barrett, J., & Tahil, A. 1987, ApJ, 319, 730
Tamura, M., Nagata, T., Sato, S., & Tanaka, M. 1987, MNRAS, 224, 413
Valleé, J. P. 1991, ApJ, 366, 450
Wilking, B. A., Lebofsky, M. J., & Rieke, G. H. 1982, AJ, 87, 695
Wilking, B. A., Lebofsky, M. J., Rieke, G. H., & Kemp, J. C. 1989, AJ, 84, 199
Wilson, T. L. 1990, Ast. Ap. Rev., 1, 141
Zweibel, E. 1987, in Interstellar Processes, ed. D. Hollenbach & H. Thronson (Boston: Reidel), 195
———. 1990, ApJ, 362, 545